ISSN (Print): 1060-6076
ISSN (Online): Applied

The Journal of African Development
2026; Vol 7: Issue 1
https://www.afea-jad.com/

Interaction Between Hydroxyapatite And Heavy Metals

Farida Fernane[1]*, Saliha Boudia[2]

[1] Natural Resources Laboratory, Mouloud Mammeri's University, Tizi ouzou, Algeria
[2] Department of Chemistry – Sciences Faculty - Mouloud Mammeri's University, Tizi ouzou, Algeria
[1]farida.fernane@ummto.dz [2]saliha.b005@gmail.com
[1] https://orcid.org/ 0000-0001-7828-884X [2] https://orcid.org/0000-0002-4079-7937
***Corresponding Author:**
Email ID : farida.fernane@ummto.dz

Cite This Paper as: Farida Fernane, Saliha Boudia (2026) Interaction Between Hydroxyapatite And Heavy Metals..The Journal of African Development l, Vol.7, No.1, 1490-1505

KEYWORDS
Cerium, hydroxyapatite, incipient wetness impregnation, ion exchange, lead.

ABSTRACT
The contamination of water and soil with heavy metals such as lead and cerium, is a major global problem. Hydroxyapatite with the stoichiometric formula Ca10(PO4)6(OH)2 could be a potential candidate for lead or cerium immobilization. This study focuses on the structural characterization of cerium and lead doped hydroxyapatite synthesized using two different methods: incipient wetness impregnation (IWI) and ion exchange (IE) under varying concentrations of Ce and Pb. X-ray diffraction (XRD), Fourier transform infrared spectroscopy (FTIR) and Scanning electron microscope (SEM) were used to understand the incorporation and/or the deposition of lead or cerium on the surface of calcined or uncalcined hydroxyapatite. Results show that cerium is deposited on the surface of the hydroxyapatite in the form of cerium hydroxy nitrate (Ce(OH)(NO3)2) for samples synthesized by IWI. However, the calcination of these samples led to the formation of CeO2. In the case of samples synthesized by ion exchange cerium is efficiently hosted in hydroxyapatite under a solid solution at a low level (<3%) but forms isolated Ce-oxide at a high level. The XRD spectra show that for powders doped with more than 0.6% Pb, characteristic peaks of PbO and Pb(NO3)2 appear respectively with the calcined and uncalcined powders prepared by the IWI method. XRD characterization showed the formation of PbHPO4 and Pb-HAP for samples synthesized by ion exchange (IE). This work indicates the excellent insertion potential of cerium or lead ions in hydroxyapatite-based matrices suitable for various applications such as energy, biomedical, catalysis, and environmental sciences. .....

1. INTRODUCTION

Hydroxyapatite (HAP) with chemical formula Ca10(PO4)6(OH)2 is the most stable calcium phosphate salt at normal temperatures and pH values between 4 and 12 [1 □3]. Hydroxyapatite is one of the biomaterials that have excellent sorption properties. Various cationic or anionic substitutions are possible due to the presence of cavities in its microstructure. Its affordability, ease of synthesis, stability, reactivity, and biocompatibility reinforce its use in several fields [4 □ 9]. On a large scale, hydroxyapatite can be easily produced, allowing for scaling up of the technology. Moreover, it can be quickly regenerated and the metals recovered without expensive processes [10]. Due to its biocompatibility, non-toxicity and osteoconductive properties, synthetic hydroxyapatite is widely used in the medical field. For this purpose, it is used for the repair and regeneration of hard bone tissue [11 □14]. Furthermore, hydroxyapatite is involved in the growth, adhesion and profiling of osteoblasts and osteoclasts [13, 14]. The crystal structure of HAP is composed of tetrahedral PO43− groups linked to Ca2+ and OH− groups [11, 12]. Different cations and anions can be integrated within this crystal structure depending on the distance between the PO43− groups [11, 15, and 16]. Cationic substitution of Ca2+ can be achieved with monovalent (Ag+ , Na+ , K+), bivalent (Mg2+, Sr2+, Zn2+, Ba2+,Pb2+, Cu2+) or trivalent (Ce3+, Sm3+, Eu3+) ions [15 – 18]. This cationic substitution gives hydroxyapatite better properties such as biocompatibility, bioactivity, non-toxicity, reduction of bone fragility and cell proliferation or growth [11, 15 - 19]. Furthermore, these ionic substitutions affect the crystallinity, crystal lattice parameters, composition and morphology of hydroxyapatite, thus leading to the development .

of a material with new properties such as chemical stability, mechanical stability, cytocompatibility, solubility and antibacterial properties [20]. Several studies report that doping with different ions increases the application range of hydroxyapatite [20 – 21]. These applications include bone tissue engineering and biomedical applications, as well as various other fields such as chromatography, fertilizers, pharmaceuticals, catalysis, gas detection, environmental pollution control, water purification processes, fluorescent lamps, and fuel cell materials [21 □ 25].

Cerium (Ce) is an abundant element on earth [16, 17, 26–29]. It is widely used in medicine for various applications such as catheters, burn treatment, and dentistry [19, 20, 29, 30]. Cerium can exist in two forms, Ce^{3+} and Ce^{4+}, and has the unique ability to change its oxidation state, which gives it antibacterial and antioxidant properties [20, 27, 29, and 30]. The cerium ion can accumulate in bones and stimulate the metabolic activity of organisms [19, 26 - 28].Therefore, characteristic advances in the field of antimicrobial vectors could be made through the development of medical device coatings using cerium-doped hydroxyapatite-based materials [19, 20, 26 - 30]. Furthermore, cerium is one of the promising candidates in the field of water treatment [31]. This is due to its stability and low toxicity compared to conventional coagulants [31]. This would minimize the risks to the environment and human health [31]. Several studies have shown that the cytotoxicity, biocompatibility and antimicrobial activity of cerium-doped hydroxyapatite depend on the synthesis method and the dopant concentration [11, 19, 28–31].

Hydroxyapatites-based adsorbents present multifunctional adsorption capacity resulting from FTIR and XRD studies related to modifications observed on hydroxyl, carbonate, phosphate and Ca^{2+} by substitution, ion exchange, complexation or precipitation [32–38]. Thus, substitution process takes place at Ca^{2+} by metal ions in form of M^{2+}, at phosphate groups by different oxyanions AsO_4^{3-}, VO_4^{3-}, etc., and at OH^- groups by monovalent anions (F^-, Cl^-, etc.) [34; 35; 37; 38]. In addition, composite HAP/organic structures can be significantly improved in terms of pollutants species than can be eliminated from aqueous solutions. Lead contamination in water and soil has been recognized as a significant environmental problem due to increasing human activities. Lead has known toxic effects on many organisms, various mineral forms, and long-term persistence in the natural environment [39; 40]. Additives based on hydroxyapatite can be used to immobilize Pb in soils [41, 42].

The aim of this study is to elucidate the structural characterization of cerium-doped hydroxyapatite and lead-doped hydroxyapatite synthesized by incipient wet impregnation (IWI) and ion exchange (IE) under different concentrations. This will enable us to elucidate the interactions between the hydroxyapatite matrix and these two metal cations during these two processes. These two processes are widely used in many fields such as catalysis to optimize the physicochemical, dielectric, and mechanical properties of hydroxyapatites before their use [4; 9; 22 and 43].

2. MATERIALS AND METHODS

The reagents required for the synthesis ($Ce(NO_3)_3.6H_2O$, 99%; $Pb(NO_3)_2$, 99% and NaOH, 99%) are Aldrich brand. The HAP powder (Ca/P = 1.649 and 99% purity) used in this study was provided by the LERISM laboratory of Paul Sabatier University in Toulouse (France).

In the incipient wetness impregnation (IWI) method, the required amount of cerium nitrate was dissolved in 7 ml of deionized water. This volume of water was previously assessed as sufficient to perfectly wet the hydroxyapatite powder. The solution is then added dropwise to 10 g of hydroxyapatite. At the end of the addition, the powder was perfectly wet. The resulting mixture is dried in an oven for 24 hours at 60°C, and then reduced to powder by gentle grinding in a mortar.

As for the ion exchange (IE) technique, it involves placing an aqueous solution of metal nitrate at a previously assessed concentration in a glass reactor. Hydroxyapatite powder is then added to the solution with constant stirring at room temperature. The pH of the reaction mixture is adjusted to 7 by adding 1M NaOH solution. After 2 hours of reaction, the suspensions are filtered through 0.45 µm filter paper.

For both methods, the concentration of metal nitrate solutions was adjusted to 0.6, 3, 7, 10 and 15 mol% (only for cerium nitrate). Each powder obtained by the IWI or IE methods was separated into two parts. The first part, uncalcined, was analyzed after drying in an oven. The second part was calcined at 600 °C in a Nabertherm L5/11/P320 static furnace before being characterized by XRD, FTIR and SEM.

The HAP phase composition and degree of crystallinity were estimated by XRD analysis using Bruker D2 X-ray diffractometer X'Pert PRO with Cu target and Kα radiation source (λ=0.15418 nm). The data were collected in 2θ ranges from 8 to 70°, with a step size of 0.02° and a counting time of 0.2s per data point. Phases are identified by comparison with

data from the Joint Committee on Power Diffraction Standards of the International Center for Diffraction Data (JCPDS-ICDD). The crystallinity degree X_C(%) corresponding to the fraction of crystalline phase of the HAP powders was evaluated by equation (1):

$$X_c = \frac{I_{300} - V_{112/300}}{I_{300}} 100 \qquad (1)$$

Where I_{300} is the intensity of (300) diffraction peak and $V_{112/300}$ the intensity of the hollow between (112) and (300) diffraction peaks of HAP.

Fourier transform infrared spectroscopy (FTIR) analyses were performed on Nicolet Impact 410 spectrometer, in the DRIFT mode without previous sample preparation. All absorption spectra were obtained by accumulation of 32 scans at 8cm^{-1} resolution in the range of 4000 –500 cm^{-1}. The SEM analyses were carried out with an accelerating high voltage (HV) of 25KV.

3. RESULTS AND DISCUSSION

A. Structure of Metal-doped HAP Synthetized by IWI Method

Results of phase composition and crystallinity degree of Ce-doped HAP by incipient wetness impregnation (IWI) are shown in Figure1 and collected in table I.

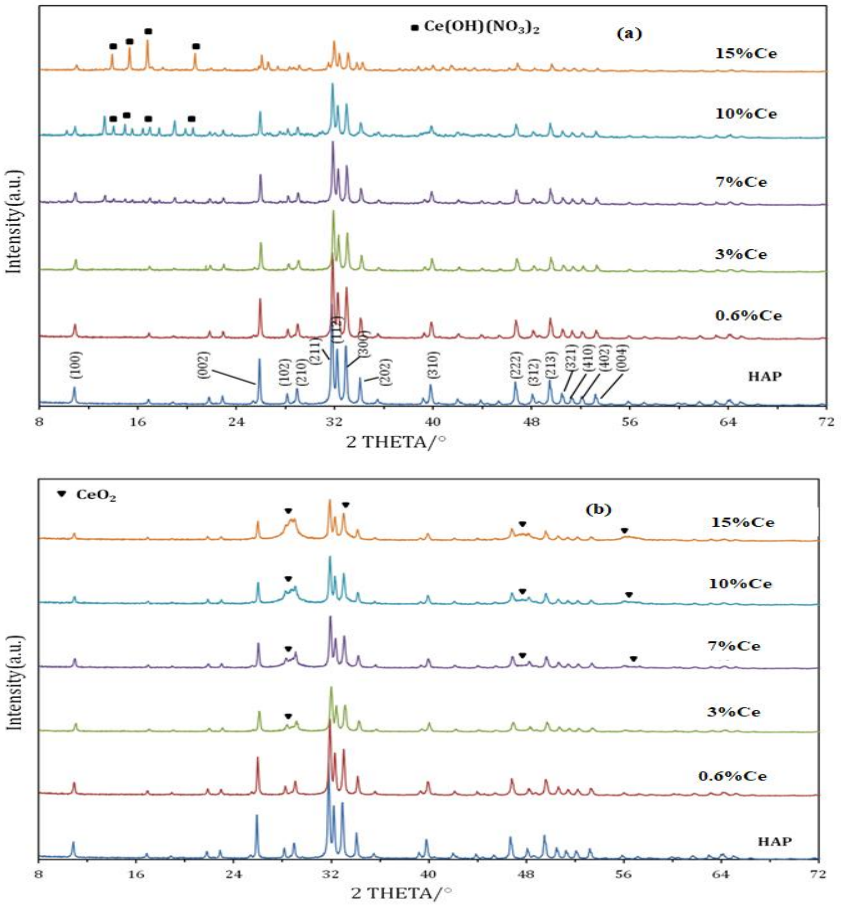

Fig. 1 XRD patterns of uncalcined (a) and calcined (b) Ce-doped HAP by IWI method

As it can be seen from XRD pattern shown in figures 1a and 1b, the peaks are characteristic to hexagonal hydroxyapatite in agreement with the JCPDS-ICDD [19; 20; 26 – 29]. The XRD pattern indicate that all the samples have the characteristic peaks in the 2θ regions of 21–29°, 32–34°,39–41°,46–54° in good agreement with the hexagonal hydroxyapatite phase. XRD spectra show that calcined and uncalcined samples containing 0.6% Ce exhibit similar XRD profiles as the initial HAP. The higher the quantity of cerium trapped, the more the intensity of the peaks increases. Beyond 0.6% Cerium, a

second phase is detected. Moreover XRD spectra show that for powders doped with more than 3% of Ce characteristic peaks of CeO_2 and $Ce(OH)(NO_3)_2$ appear respectively with calcined and uncalcined powders.

TABLE I Crystallinity degree of Ce-doped HAP samples prepared by IWI with different amount of Ce

Samples	Crystallinity levels X_C (%)	
	Uncalcined Samples	Calcined Samples
Initial HAP	95.12	95.12
0.6% Ce IWI	89.14	87.23
3% Ce IWI	87.46	83.52
7% Ce IWI	86.25	88.06
10% Ce IWI	82.54	80.28
15% Ce IWI	77.14	72.29

The variation in the intensity of the diffraction peaks of the two phases creates a broadening of the observed lines. This leads to a reduction in the crystallinity degree of the samples relative to the quantity of cerium trapped (Table I). The incorporation of cerium ions slightly broadens the diffraction peaks of the initial hydroxyapatite. Furthermore, we notice that the relative intensity of all diffraction peaks decreases slightly as the amount of cerium incorporated into the hydroxyapatite structure increases. This could be related to the substitution mechanism between Ca^{2+} ions and those of cerium as reported by several previous works [30; 44 and 45]. Indeed, the similarity of the ionic radii of Ce^{3+} (1.04 Å) and Ce^{4+} (0.97 Å) compared to Ca^{2+} (1.06 Å) may favor this substitution within the hydroxyapatite lattice [27; 30; 44 and 45].

In the case of lead, the X-ray diffraction (XRD) spectra shown in Figure 2 indicate that, for powders doped with more than 0.6 % Pb, characteristic peaks of PbO and $Pb(NO_3)_2$ appear in the calcined and uncalcined powders respectively. A second phase is detected when this percentage exceeds 0.6%. In the case of the uncalcined samples (Figure 2b), characteristic peaks of lead nitrate appear, corresponding to the monoclinic structure of $Pb(NO_3)_2$. In the case of the calcined samples (Figure 2a), a lead oxide phase appears.

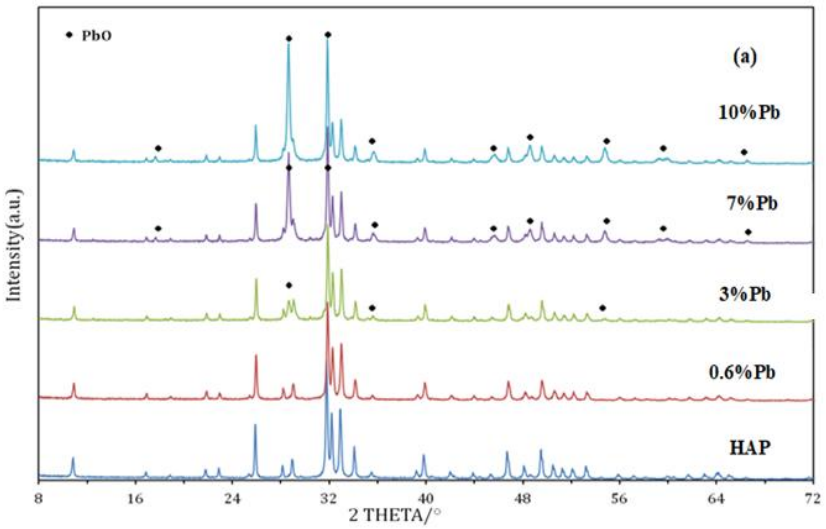

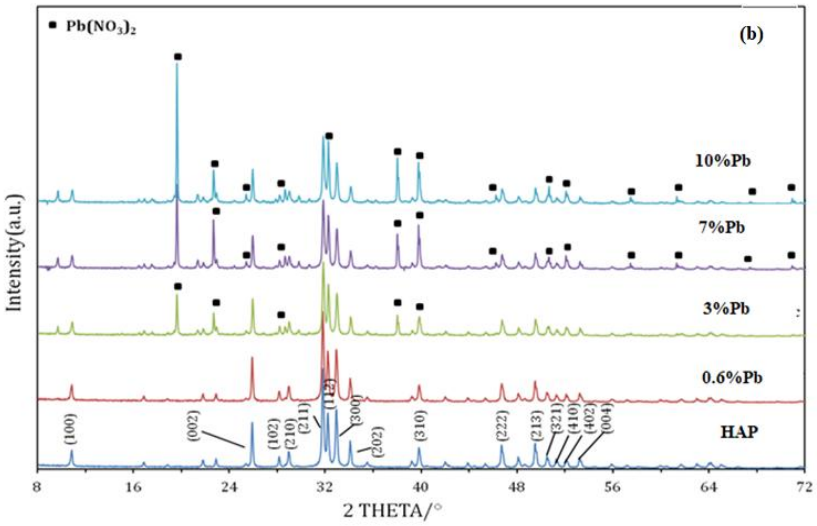

Fig. 2 XRD patterns of calcined (a) and uncalcined (b) Pb-doped HAP by IWI method

The degree of crystallinity shown in Table II confirms the effect of the amount of Pb and calcination on the level of crystallinity.

TABLE II Crystallinity degree of Pb-doped HAP samples prepared by IWI with different amount of Pb

Samples	Crystallinity level X_C (%)	
	Uncalcined Samples	Calcined Samples
Initial HAP	95.12	95.12
0.6% Pb	85.02	85.13
3% Pb	84.56	83.78
7% Pb	83.87	82.71
10% Pb	82.36	79.08

These results show that, relative to the initial hydroxyapatite, the degree of crystallinity decreases as the amount of lead increases. Previous works suggest that crystallinity is detrimental to the substitution of Pb^{2+} ions by Ca ions in hydroxyapatite (32 – 34, 37 and 46).

The FTIR spectra of the initial HAP and cerium-doped HAP samples using the IWI technique are shown in Figure 3. These spectra are congruent and correspond to the absorption spectra of a hydroxyapatite. Therefore, the main peaks observed around 564cm^{-1}, 604cm^{-1}, 961cm^{-1}, 1033cm^{-1} and 1090cm^{-1} are related to the tetrahedral PO_4^{3-} groups characteristic of hydroxyapatite [30, 44 - 48]. However, compared to the initial HAP, the uncalcined samples (containing 3 to15% of Ce) exhibit additional peaks at 1445, 1345, 1306, 875 and 750cm^{-1}, which can be attributed to nitrate vibration in the NO band [31-33]. These peaks increase with the amount of cerium fixed. But these peaks no longer appear in the case of calcined samples. These results confirm the value of calcination in the hydroxyapatite doping process, as mentioned in several studies [21; 30 - 31]. These FTIR results are in good agreement with the XRD one. Cerium oxide did not show IR bands as is known for the metal oxide.

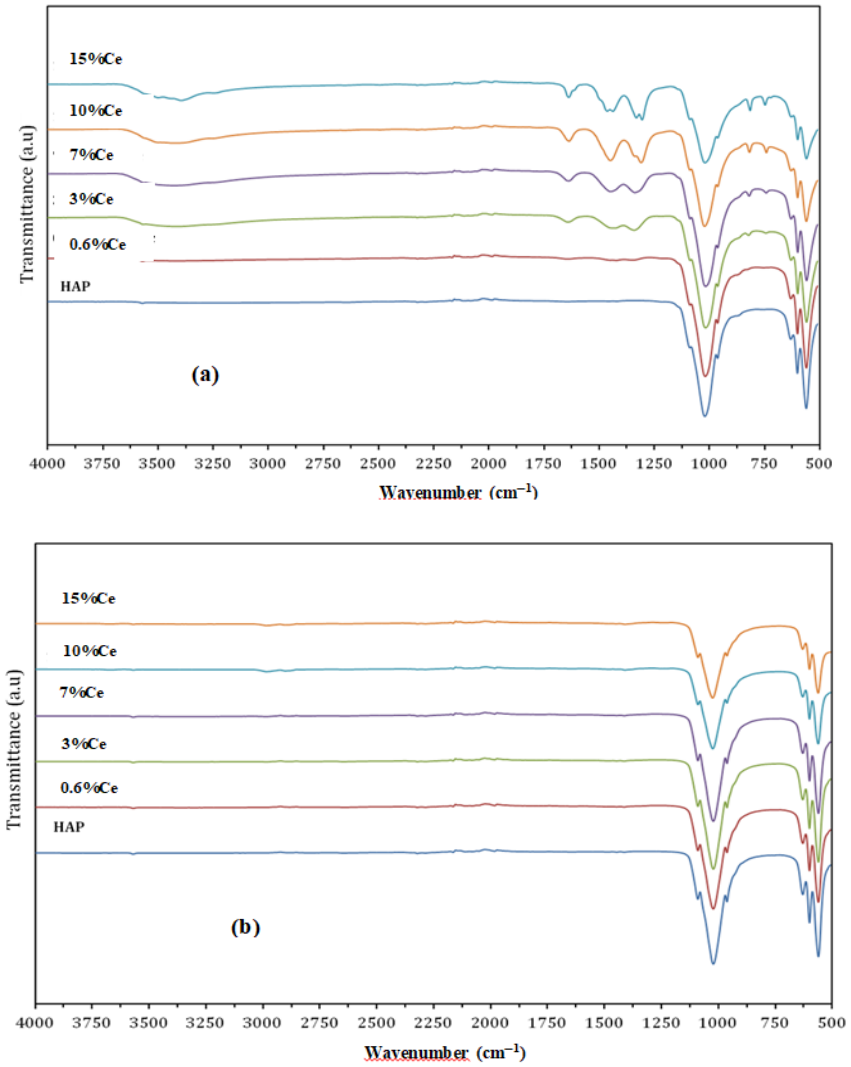

Fig. 3 FTIR spectra of uncalcined (a) and calcined (b) Ce-doped HAP by IWI methods

The FTIR spectra of initial HAP and Pb-doped HAP are shown in Figures 4a and 4b respectly for calcined and uncalcined powder HAP .The FTIR spectra of the samples are stackable and correspond to the expected absorption spectra for the hydroxyapatite.The spectrum reveals the presence of the vibrational modes corresponding to phosphate and hydroxyl groups.The 3570 and 628 cm^{-1} bands are observed, which correspond respectively to the symmetrical valence vibrations and liberation movements of OH^- ions. The intense absorption bands at (1089, 1024) and 968cm^{-1} are due to the P—O asymmetric and symmetrical elongation mode respectively. Two strong bands at 599 and 560cm^{-1} are assigned to the O—P—O antisymmetric deformation mode. These are the main characteristic bands of HAP [40; 46; 49 and 52]. The uncalcined samples with 3%, 7% and 10% of Pb present a band at 1345 cm^{-1} which is characteristic of the NO_3 groups derived from the nitrated residues (Figure 4b). In the case of same samples calcined at 600°C (Figure 4a) band associated with nitrate groups disappears. These results confirm the value of calcination in the hydroxyapatite doping process, as mentioned in several studies [21; 46 and 52].

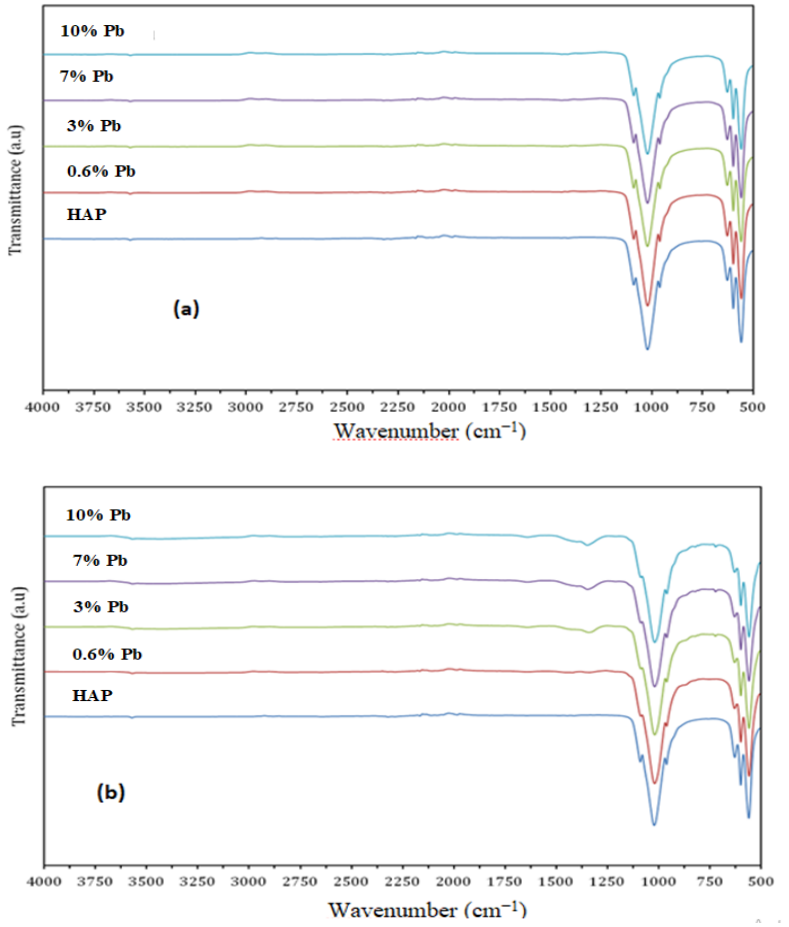

Fig. 4 FTIR spectra of calcined (a) and uncalcined (b) Pb-doped HAP by IWI method

Figure 5 shows SEM images taken on calcined sample HAP-IWI-10% Ce. The images show presence of white particles as a randomly distributed aggregate that would be CeO_2. However at higher magnification these aggregates appear to be a mixture of small agglomerated particles.

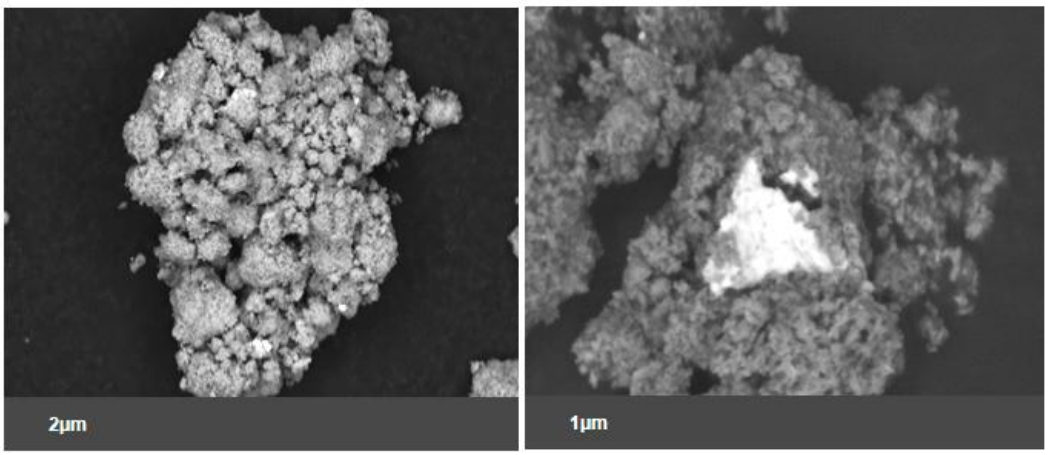

Fig. 5 SEM micrograph of calcined 10%Ce-doped HAP by IWI method

Figure 6 gathers the SEM micrographs of calcined HAP 10% lead-doped powder. We observe white particles that tend to form agglomerates. A magnification of the image shows a crystal in quadratic form characteristic of the litharge (PbO) [40]. The crystal appears elongated, with a size close to 8 to 10 µm in length and a few hundred nanometers in width. These results are similar to those presented in several works [33; 40; 41; and 49].

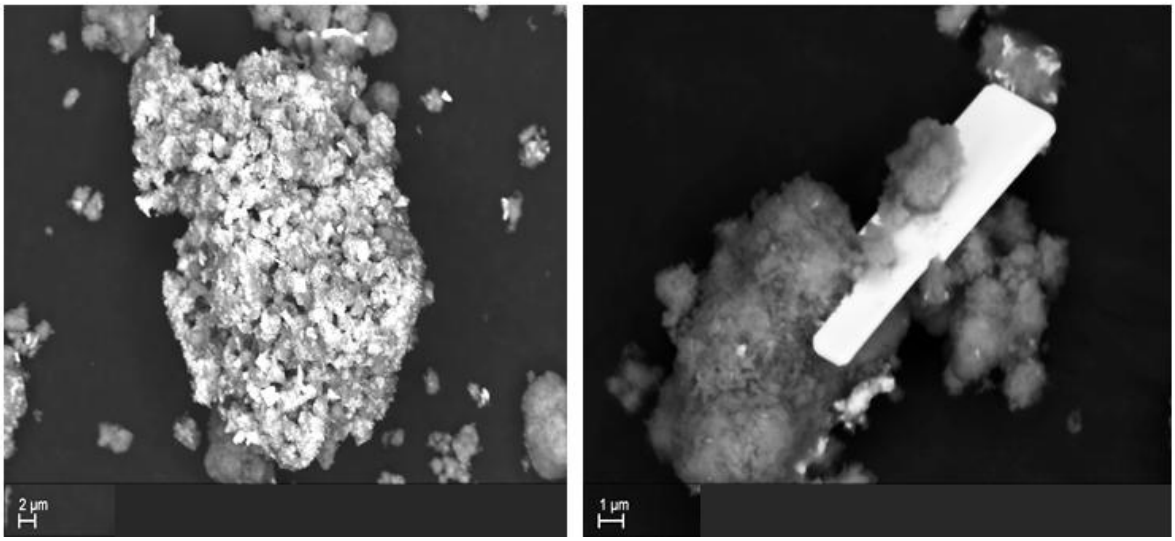

Fig. 6 SEM micrograph of calcined 10% Pb-doped HAP by IWI method

B. Structure of Metal-doped HAPSynthetized by IE Method

The XRD results are shown in figure 7. They indicate that all samples have the characteristic peaks in good agreement with the hexagonal phase of HAP and no obvious phase changes were observed. The diagrams of calcined and uncalcined Ce-doped HAP samples also show sharp peaks but of lesser intensity.

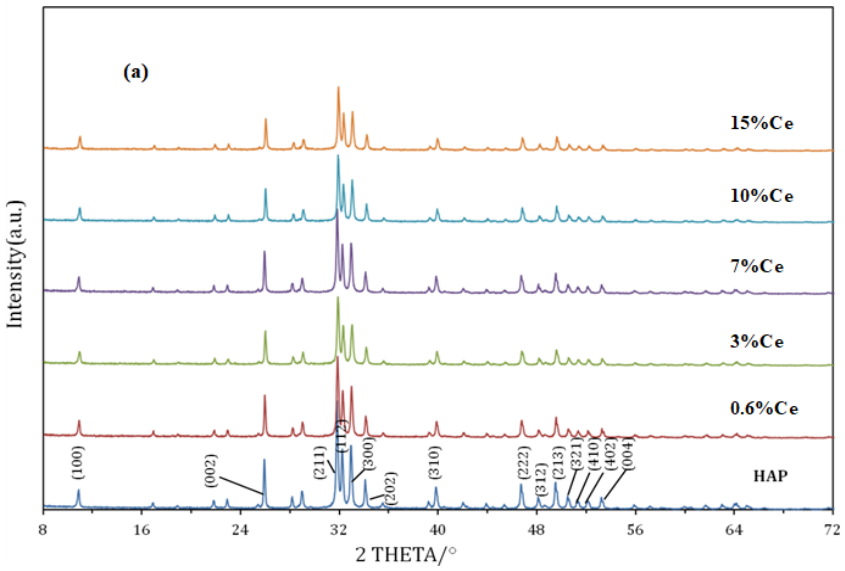

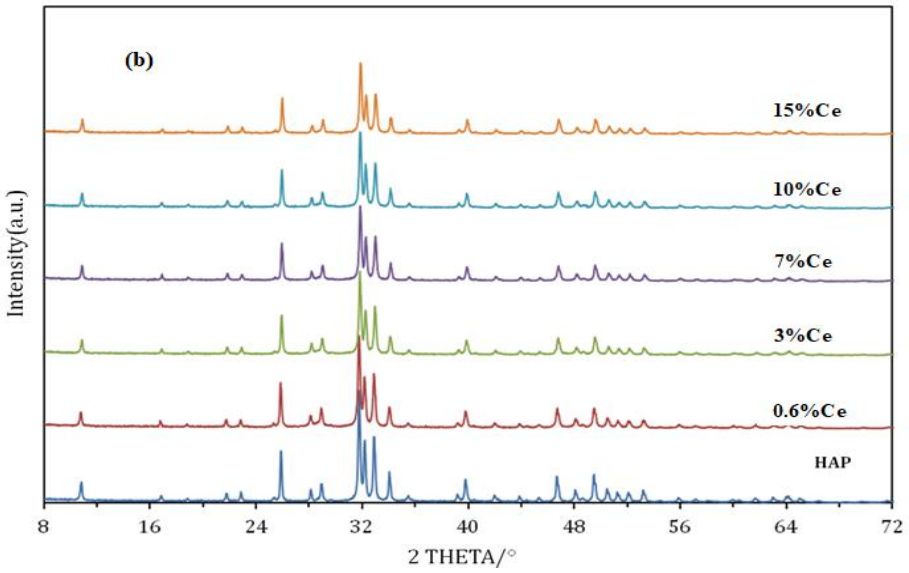

Fig. 7 XRD patterns of uncalcined (a) and calcined(b) Ce-doped HAP by ion exchange (IE) method

Figures 8 show diffractograms of Pb-doped HAP by ion exchange for different percentages of Pb(II) used.The main peaks at 26°, 32°, 32.4° and 33.2° found for initial hydroxyapatite decrease as lead concentration increases. At the same time the increase in initial Pb concentration of solution leads the formation of new peaks corresponding two phases. The first one being the $PbHPO_4$ phase with the characteristic peaks at 13.5°, 14.3°, 27.3° and 29.2°. The second one is Pb-HAP with peaks at 18.4°, 22.5° and 30.2°. The figure 8(b) shows that PbHAP and $PbHPO_4$ phases disappear and lead present in the sample turns into PbO during heat treatment. The intensity of peaks shows that the increase of Pb concentration in initial solution leads to an increase in the intensity of PbO diffractogram. Similar results have b een reported by several authors [32; 34; 37;39; 40; 46; 50;51 and 52].

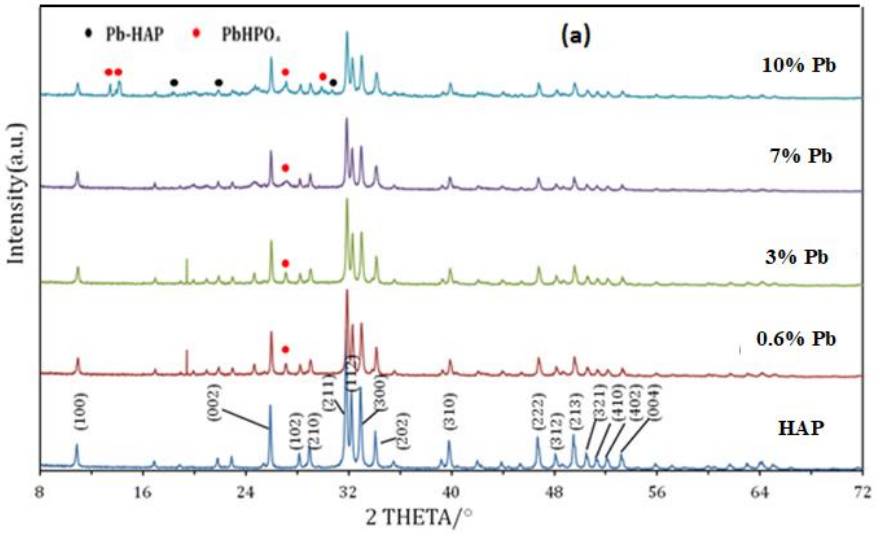

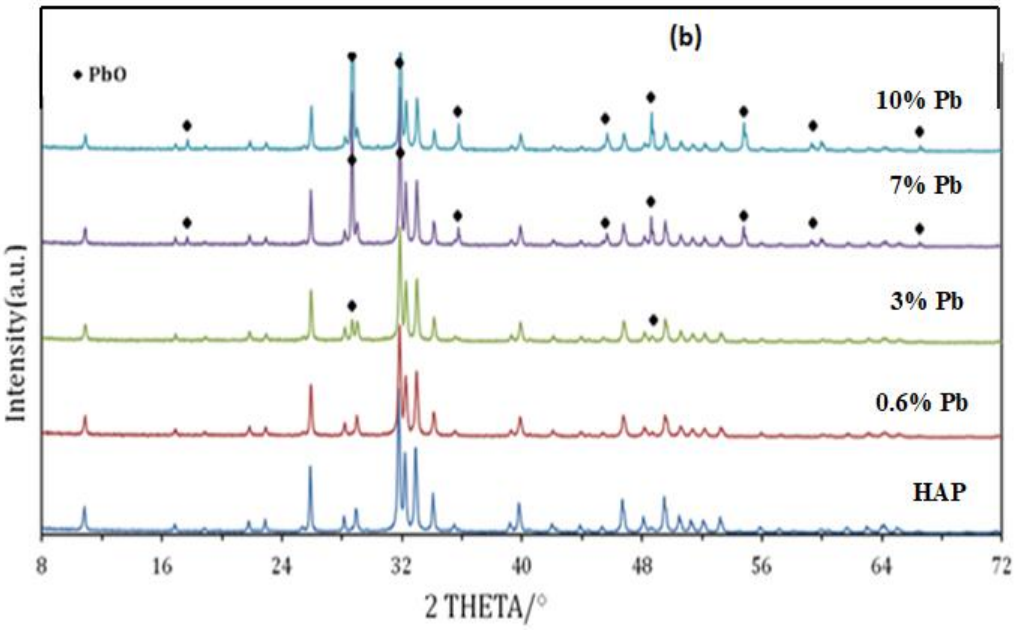

Fig. 8 XRD patterns of uncalcined (a) and calcined(b) Pb-doped HAP by ion exchange (IE) method

Figure 9 shows FTIR spectra of uncalcined and calcined Ce-doped HAP by ion exchange. It can be noted that 474 (O–P–O bonding mode), 960 (P–O symmetric stretching), 1035 and 1101 cm^{-1} (P–O asymmetric stretching) IR bands can be attributed to the internal vibrations in the PO_4^{3-} groups in the apatitic structure [27 - 30]. Furthermore the maximum forces of the O—H and P—O bonds decrease with the increased amount of cerium fixed. The weakening of P—O bands could result from the introduction of Ce^{4+}/Ce^{3+} ions and the subsequent alteration of binding force between the ions leading to the weakening of the P—O and O—P—O vibrations [33- 36].

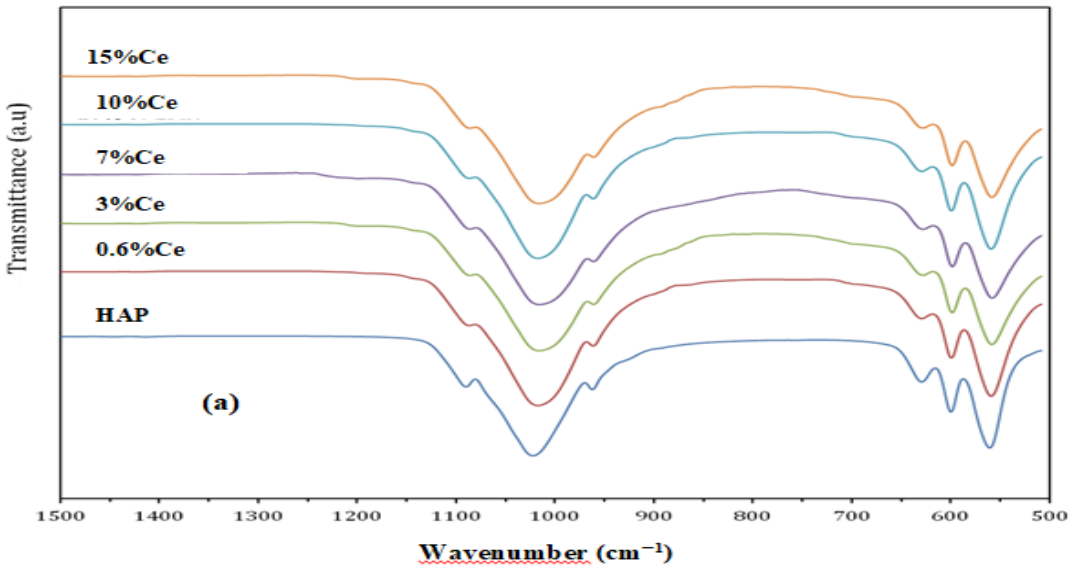

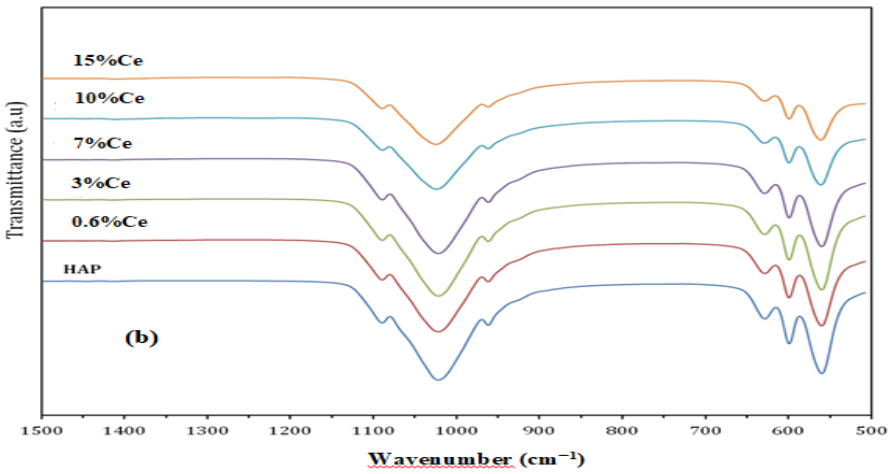

Fig. 9 FTIR spectra of uncalcined (a) and calcined (b) Ce-doped HAP by IE method

Figure 10 shows FTIR spectra of uncalcined and calcined Pb-doped HAP by ion exchange. On spectra of non-calcined powders (Figure 10a) composed of 7% and 10% Pb nitrate bands at 1345 and 740 cm^{-1} are detected. After calcinations (Figure 10b) all the spectra are super imposable and we don't observe the presence of any band after doping with lead at different concentrations.

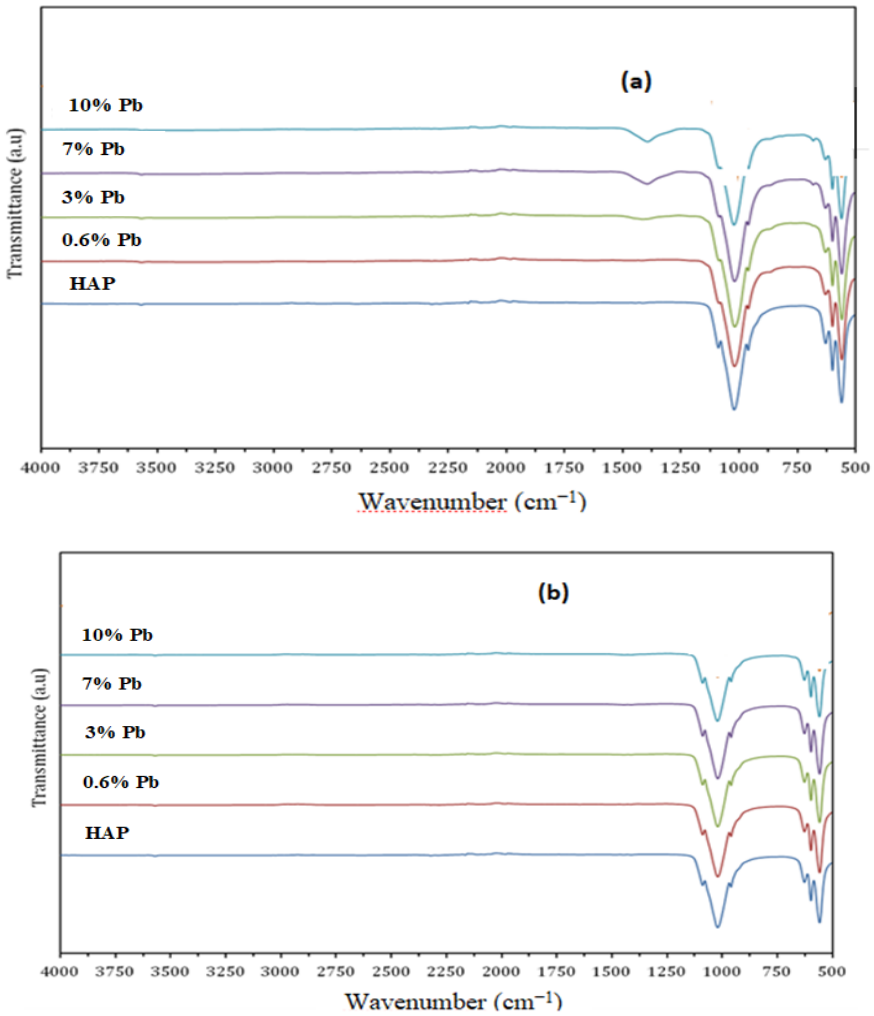

Fig. 10 FTIR spectra of uncalcined (a) and calcined (b) Pb-doped HAP by IE method

Figure 11 shows an SEM image taken on calcined 10% Ce doped HAP synthesized by ion exchange method. The image shows the agglomeration of particles and a uniform distribution of cerium on the surface of hydroxyapatite. This agglomeration process cannot be avoided because in the calcination step (600°C) HAP particles tend to sinter into agglomerates made of polycrystals [19, 20].

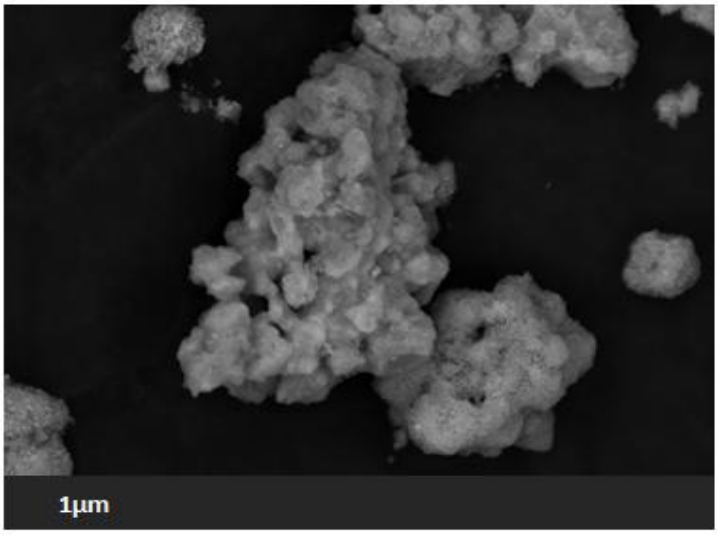

Fig. 11 SEM micrograph of calcined 10% Ce-doped HAP synthetized by IE method

The observations made by SEM (Figure 12) on calcined Pb-doped HAP by ion exchange sample show bright spots distributed randomly on the surface of the hydroxyapatite. For a larger magnification these spots consist of small crystallites in order of a few microns well agglomerated. These crystallites have different shapes. However a prismatic crystal with an hexagonal pyramid can be considered as a characteristic termination of the $Pb_xCa_{5-X}(PO_4)_3OH$ solids as suggested by several previous works [40; 46; 49; 51and 52].

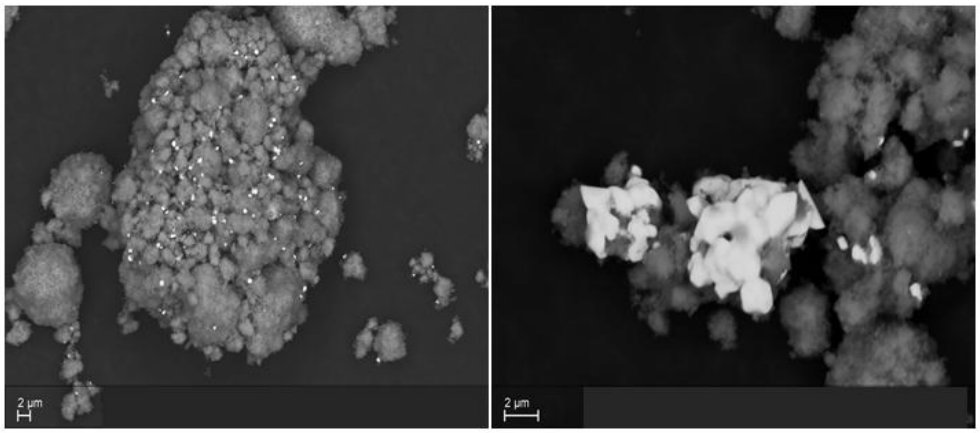

Fig. 12 SEM micrograph of calcined 10% Pb-doped HAP synthetized by IE method

C. Discussion

The results of the samples synthesized by IWI showed that cerium was deposited on the surface of hydroxyapatite in the

form of cerium hydroxy nitrate ($Ce(OH)(NO_3)_2$). Indeed, nitrate bands were observed. They were visible on the FTIR spectra. However, calcination of these samples led to the formation of CeO_2, as confirmed by XRD spectra and SEM observations. In the case of samples synthesized by ion exchange, we observed two different mechanisms related to the amount of cerium ions initially incorporated. For quantities below 3%, cerium is introduced into the hydroxyapatite structure in the form of a solid solution. For initial quantities of 7, 10 and 15%, cerium forms isolated cerium oxide.

The XRD results show that the crystallinity of HAP decreases as the amount of Ce(III) incorporated increases. This reflects a possible substitution mechanism between the Ca^{2+} ions of HAP and cerium within the HAP lattice. This substitution is made easier because the ionic radii of cerium (1.04 Å for Ce^{3+} and 0.97 Å for Ce^{4+}) are pretty similar to those of Ca^{2+} (1.06 Å). Several authors have reported similar results when studying the mechanisms of cerium doping of hydroxyapatite [19, 26 – 30 and 33].

Several studies have highlighted the link between the cationic substitution of Ca^{2+} ions in the HAP and the improved properties of medical implants based on hydroxyapatite doped, in particular, with cerium. These properties include biocompatibility, bioactivity, non-toxicity, reduced bone fragility, and cell proliferation or growth [17, 20, 26, 27, 30, and 33]. Furthermore, when used as a coating, doped hydroxyapatite can promote interfacial bonding with implants, prostheses, or surrounding tissues [33 - 36].

In the case of lead, samples synthesized by dry impregnation (IWI), the XRD results showed that lead is deposited on the surface of hydroxyapatite in the form of lead nitrate. Thus, nitrate bands were observed on the FTIR spectra. Calcination of these samples led to the formation of PbO. For samples synthesized by ion exchange (IE) XRD showed the formation of two phases which are $PbHPO_4$ and Pb-HAP. However, the SEM observations showed the presence of crystallites of different shapes with the demonstration of a prismatic crystal characteristic of solids [$Pb_xCa_{5-x}(PO_4)_3OH$].

Several studies have shown that heavy metal-doped hydroxyapatite (HAP) exhibit varying adsorption capacities for heavy metals depending on factors like doping level, solution pH, and the specific heavy metal [32; 34; 37; 39; 40; 46; 50;51 and 52]. Numerous studies have presented specific results of hydroxyapatite doped with Cu^{2+}, Mg^{2+}, Zn^{2+}, Ag^{+}, and many other ions (Simona et al. 2018; Anushika et al. 2019; Kazuki et al. 2022; Nasrallah et al. 2022; Bast et al. 2024; Duta et al. 2024). In this regard, they mentioned that doped hydroxyapatite slightly modified the characteristic peaks. The crystal structure has been affected by the doping agent. Moreover, the doping ion can lead to distortions in the crystal and lattice parameters, which can have a significant impact on the overall structure and properties of the material. Also, the percentage of crystallite size and crystallinity is reduced. The microstructure, lattice parameters, crystallinity, grain size, crystal morphology, thermal stability, and solubility of hydroxyapatite are all influenced by the concentration, size, and type of ionic doping agents.

Ankita et al.(2025) presented hydroxyapatite as a promising candidate for sustainable wastewater treatment. The study described the innovations using wastes for the synthesis of HAP by diverse methods like wet, dry, high-temperature, and hybrid methods, offering flexibility and adaptability in tailoring HAP material to particular applications. This review paper provides insights on a comprehensive overview of research works on HAP-based wastewater treatment, extending its potential to address the issue of heavy metal contamination and highlighting the universal principle 'One Health' - the health of the ecosystem and its parts (Ankita et al.2025).

4. CONCLUSIONS

The results of this work show the great potential of Ce(III) and Pb(II) ions to be doped in a hydroxyapatite matrix, using either in situ wet impregnation or ion exchange techniques. Both techniques can be adapted to various applications, including biomedical sciences, energy, catalysis, and environmental sciences. In light of the results of this study, it appears that the IWI technique is better suited to the doping of hydroxyapatite for use in catalysis and the regeneration of hard bone tissue. By contrast, hydroxyapatite prepared using the IE method would be more suitable for the treatment of water or soil contaminated with heavy metals.

Finally, we can conclude that the IWI and EI techniques tested in this study for doping hydroxyapatite could be recommended for the development of a low-cost material for biomedical and environmental applications..

References

1. G. Molino, M. C. Palmieri, G. Montalbano, S. Fiorilli and C. Vitale-Brovarone. Biomimetic and mesoporous nanohydroxyapatite for bone tissue application: A short review. Biomedical Materials.15(2):022001(2020).

2. A. A. Majhooll, I., Zainol, C. N. A., Jaafar, A., Ha, M. Z., Hassan, M., Mudhafar, A. A. Majhool and A. Asaad. A brief review on biomedical applications of hydroxyapatite use as fillers in polymer. J. Chem.13:112-119 (2019).

3. Chatterjee,T; Ghosh,M;Maji,M;Pradhan,SK; Meikap,A.K. Study of microstructural and electrical properties of silver substituted hydroxyapatite for drug delivery applications. Mater. Today Commun. 31, 103360 (2022)

4. Mehdi Arab , Panteha Behboodi , Adrine Malek Khachatourian , Ali Nemati. Enhanced mechanical properties and biocompatibility of hydroxyapatite scaffolds by magnesium and titanium oxides for bone tissue applications. Heliyon 10 e33847 (2024).

5. S. Pai, S. M Kini, R. Selvaraj, A. Pugazhendhi. A review on the synthesis of hydroxyapatite, its composites and adsorptive removal of pollutants from wastewater, J. Water Proc. Eng. 38, 101574 (2020).

6. V. Rodríguez-Lugo, et al., Wet chemical synthesis of nanocrystalline hydroxyapatite flakes: effect of pH and sintering temperature on structural and morphological properties, R. Soc. Open Sci. 5 (8), 180962 (2018).

7. I.-H. Lee, J.-A. Lee, J.-H. Lee, Y.-W. Heo, J.-J. Kim, Effects of pH and reaction temperature on hydroxyapatite powders synthesized by precipitation, J. Korean Ceram. Soc. 57 (1) 56–64, (2020).

8. A. Biedrzycka, E. Skwarek, U.M. Hanna, Hydroxyapatite with magnetic core: synthesis methods, properties, adsorption and medical applications, Adv. Colloid Interface Sci. 291, 102401, (2021).

9. Liviu Duta, Valentina Grumezescu. The effect of doping on the electrical and dielectrical properties of hydroxyapatite for medical applications: from powders to thin films. Materials 17, 640 (2024).

10. Ibrahim, M.; Labaki, M.; Giraudon, J.-M.; Lamonier, J.-F. Hydroxyapatite, a multifunctional material for air, water and soil pollution control: A review. J. Hazard. Mater. 383, 121139 (2020).

11. Tite, T.; Popa, A.-C.; Balescu, L.M.; Bogdan, I.M.; Pasuk, I.; Ferreira, J.M.F.; Stan, G.E. Cationic Substitutions in Hydroxyapatite:Current Status of the Derived Biofunctional Effects and Their In Vitro Interrogation Methods. Materials, 11, 2081(2018).

12. Eliaz, N.; Metoki, N. Calcium Phosphate Bioceramics: A Review of Their History, Structure, Properties, Coating Technologies and Biomedical Applications. Materials, 10, 334 (2017).

13. Sima, L.E.; Stan, G.E.; Morosanu, C.O.; Melinescu, A.; Ianculescu, A.; Melinte, R.; Neamtu, J.; Petrescu, S.M. Differentiation of mesenchymal stem cells onto highly adherent radio frequency-sputtered carbonated hydroxylapatite thin films. J. Biomed. Mater.Res. Part A, 95, 1203–1214 (2010).

14. Wang, P.; Zhao, L.; Liu, J.; Weir, M.D.; Zhou, X.; Xu, H.H.K. Bone tissue engineering via nanostructured calcium phosphate biomaterials and stem cells. Bone Res., 2, 14017 (2014).

15. Sahu, T.; Bisht, S.S.; Ranjan, D.K.; Kerkar, S. Nanoceria: Synthesis and Biomedical Applications. Curr. Nanosci., 9, 588–593 (2013).

16. Ouyang, Y.; Xie, Y.; Tan, S.; Shi, Q.; Chen, Y. Structure and antibacterial activity of Ce3+ exchanged montmorillonites. J. Rare Earths, 27, 858–863 (2009).

17. Predoi, D.; Iconaru, S.L.; Predoi, M.V.; Groza, A.; Gaiaschi, S.; Rokosz, K.; Raaen, S.; Negrila, C.C.; Prodan, A.-M.; Costescu, A.; et al. Development of Cerium-Doped Hydroxyapatite Coatings with Antimicrobial Properties for Biomedical Applications. Coatings, 10, 516 (2020).

18. Iconaru, S.L.; Groza, A.; Gaiaschi, S.; Rokosz, K.; Raaen, S.; Ciobanu, S.C.; Chapon, P.; Predoi, D. Antimicrobial Properties of Samarium Doped Hydroxyapatite Suspensions and Coatings. Coatings, 10, 1124 (2020).

19. Ciobanu, C.S.; Nica, I.C.; Dinischiotu, A.; Iconaru, S.L.; Chapon, P.; Bita, B.; Trusca, R.; Groza, A.; Predoi, D. Novel Dextran Coated Cerium Doped Hydroxyapatite Thin Films. Polymers, 14, 1826 (2022).

20. Daniela Predoi, Simona Liliana Iconaru, Mihai Valentin Predoi, Andreea Groza, Sofia Gaiaschi, Krzysztof Rokosz , Steinar Raaen , Catalin Constantin Negrila , Alina-Mihaela Prodan, Adrian Costescu, Monica Luminita Badea and Patrick Chapon . Development of Cerium-Doped Hydroxyapatite Coatings with Antimicrobial Properties for Biomedical Applications. Coatings, 10, 516, (2020).

21. D. E. Radulescu, O. R. Vasile, E. Andronescu and A. Ficai. Latest research of doped hydroxyapatite for bone tissue engineering. International Journal of Molecular Sciences. 24(17):13157 (2023).

22. Ercan, J; Kaygili,O; Kayed,T; Bulut,N; Tombuloglu,H; Ince,T; Ahmari, F.A; Kebiroglu,H; Ates,T; Almofleh,A; et al.

Structural, spectroscopic, dielectric, and magnetic properties of Fe/Cu co-doped hydroxyapatites prepared by a wet-chemical method. Phys.B Condens.Matter. 625, 413486 (2022).

23. Nasrallah, D.A; Ibrahim, M.A. Enhancement of physic-chemical, optical, dielectric and antimicrobial properties of polyvinyl alcohol/carboxymethyl cellulose blend films by addition of silver doped hydroxyapatite nanoparticles. J.Polym.Res. 29, 86 (2022)
24. Helen,S; Ruban Kumar,A. Study of structural, mechanical and dielectrical properties of ions doped apatite for antibacterial activity. Mater. Chem. Phys. 237, 121867 (2019)
25. Anushika; Sharma, P.; Trivedi, A.; Begam, H. Synthesis and characterization of pure and titania doped hydroxyapatite. Mater. Today Proc. 16, 302–307 (2019).
26. T. Ivankovic , A.Zuzic, I.Urlic, V.Alessandra Gobbo, B.Dadic, T.Sandblom, S.Zakeri, M.Virpinen, I. Goic-Barisic, J.Hrenovic, J.Massera, E. Levanen , A. Ressler. Cerium, copper, gallium, manganese and silver substituted hydroxyapatite: cytotoxicity and antibacterial activity toward multidrug-resistant clinical isolates. Journal of Hazardous Materials Advances 18, 100731(2025)
27. C.S Ciobanu, C.L Popai, D.Predoi. Cerium doped hydroxyapatite nanoparticles synthesized by coprecipitation method. J. Serb. Chem. Soc. 81 (0) 1–14 (2016)
28. Kubiak-Mihkelsoo, Z.; Kostrz¸ ebska, A.; Błaszczyszyn, A.; Pitułaj, A.; Dominiak, M.; Gedrange, T.; Nawrot-Hadzik, I.; Matys, J.; Hadzik, J. Ionic Doping of Hydroxyapatite for Bone Regeneration: Advances in Structure and Properties over Two Decades—A Narrative Review. Appl. Sci., 15, 1108 (2025).
29. De Lama-Odría, M.d.C.; Valle, L.J.d.; Puiggalí, J. Lanthanides-Substituted Hydroxyapatite for Biomedical Applications. Int. J. Mol. Sci., 24, 3446 (2023).
30. Iconaru, S.L.; Predoi, M.V.; Chapon, P.; Gaiaschi, S.; Rokosz, K.; Raaen, S.; Motelica-Heino, M.; Predoi, D. Investigation of Spin Coating Cerium-Doped Hydroxyapatite Thin Films with Antifungal Properties. Coatings, 11, 464 (2021).
31. Osra, F.A. Cerium as an Efficient Coagulant for Phosphorus Removal from Wastewater. Sustainability, 17, 1862 (2025).
32. Bernalte, E.; Kamieniak, J.; Randviir, E.P.; Bernalte-García, Á.; Banks, C.E. (2019)The preparation of hydroxyapatite from unrefined calcite residues and its application for lead removal from aqueous solutions. RSC Adv. 9, 4054–4062
33. Brazdis, R.I.; Fierascu, I.; Avramescu, S.M.; Fierascu, R.C. (2021) Recent Progress in the Application of Hydroxyapatite for the Adsorption of Heavy Metals from Water Matrices. Materials.14, 6898
34. Hariani, P.L.; Riyanti, F.; Fatma, F.; Rachmat, A.; Herbanu, A. (2020)Removal of Pb(II) using Hydroxyapatite from Golden Snail Shell (Pomacea canaliculata L.) Modified with Silica. Molekul. 15, 130–139
35. Hernández-Cocoletzi, H.; Salinas, R.A.; Águila-Almanza, E.; Rubio-Rosas, E.; Chai, W.S.; Chew, K.W.; Mariscal-Hernández, C.; Show, P.L. (2020)Natural hydroxyapatite from fishbone waste for the rapid adsorption of heavy metals of aqueous effluent. Environ. Technol. Innov. 20, 101109
36. Ibrahim, M.; Labaki, M.; Giraudon, J.-M.; Lamonier, J.-F. (2020)Hydroxyapatite, a multifunctional material for air, water and soil pollution control: A review. J. Hazard. Mater. 383, 121139
37. Omar, S.; Muhamad, M.S.; Chuan, L.T.E.; Rudi, N.N.; Hamidon, N.; Hamid, N.H.A.; Harun, H.; Sunar, N.M.; Ali, R. (2020) Effect of Hydroxyapatite (HAp) Adsorbent dosage towards lead removal. Int. J. Emerg. Trends Eng. Res. 8, 201–205.
38. Ramdani, A.; Taleb, Z.; Guendouzi, A.; Kadeche, A.; Herbache, H.; Mostefai, A.; Taleb, S.; Deratani, A. (2020) Mechanism study of metal ion adsorption on porous hydroxyapatite: Experiments and modeling. Can. J. Chem. 98, 79–89.
39. Mobasherpour,I.; Salahi, E. and Pazouki, M. (2012)Comparative of the removal of Pb2+, Cd2+ and Ni2+ by nano crystallite hydroxyapatite from aqueous solutions: adsorption isotherm study. Arabian Journal of Chemistry, vol. 5, no. 4, pp. 439–446
40. Inian Zhu, Bin Huang, Zongqiang Zhu, Huili Liu, Xin Zhao and Meina Liang. (2016)Characterization, dissolution and solubility of the hydroxypyromorphite–hydroxyapatite solid solution [(PbxCa1−x)5(PO4)3OH] at 25°C and pH 2–9. Geochem Trans 17:2,

41. He, M.; Shi, H.; Zhao, X.; Yu, Y.; Qu, B. (2013)Immobilization of Pb and Cd in contaminated soil using nano-crystallite hydroxyapatite. Procedia Environ. Sci., 18, 657–665

42. Rosskopfová, O.; Viglašová, E.; Galamboš, M.; Daňo, M.; Tóthová, D. (2023)The Removal of Pertechnetate from Aqueous Solution by synthetic hydroxyapatite: The role of reduction reagents and organic ligands. Int. J. Environ. Res. Public Health. 20, 3227.

43. Bast Ahmad , Tankut Ates, Bahroz Kareem Mahmood , Rebaz Obaid Kareem , Serhat Keser , Niyazi Bulut, Omer Kaygili. The effects of pH on the morphology and structural properties of Er/Yb codoped hydroxyapatite. Journal of Physical Chemistry and Functional Materials Volume 7, Issue 1 11-16 (2024).

44. P.Phataia, C.M.Futalan, S.Utara, P.Khemthong, S.Kamonwannasit. Structural characterization of cerium-doped hydroxyapatite nanoparticles synthesized by an ultrasonic-assisted sol-gel technique. Results in Physics 10956–963 (2018).

45. Ciobanu. G, Bargan.A. M, Luca.C. New cerium (IV)-substituted hydroxyapatite nanoparticles: Preparation and characterization. Ceramics International 4112192–1220 (2015) Ceramics International Volume 41, Issue 9, Part B, 12192-12201(2015).

46. Simona Liliana Iconaru, Mikael Motelica-Heino , Regis Guegan , Mircea Beuran ,Adrian Costescu, Daniela Predoi. (2018) Adsorption of Pb (II) Ions onto Hydroxyapatite Nanopowders in Aqueous Solutions. Materials, 11, 2204.

47. Predoi, D.; Iconaru, S.L.; Predoi, M.V.; Motelica-Heino, M.; Guegan, R.; Buton, N. Evaluation of Antibacterial Activity of Zinc-Doped Hydroxyapatite Colloids and Dispersion Stability Using Ultrasounds. Nanomaterials, 9, 515 (2019).

48. Leu Alexa, R.; Cucuruz, A.; Ghit,ulic ˘a, C.-D.; Voicu, G.; Stamat, L.-R.; Dinescu, S.; Vlasceanu, G.M.; Stavarache, C.; Ianchis, R.; Iovu, H.; et al. 3D Printable Composite Biomaterials Based on GelMA and Hydroxyapatite Powders Doped with Cerium Ions for Bone Tissue Regeneration. Int. J. Mol. Sci., 23, 1841 (2022).

49. Novikova, S.; Gilev, A.; Brickmans, A.; Priymak, I.; Shlyk, D.; Nesterova, O.; Egorin, A. (2025) The potential of hydroxyapatite for the remediation of lead-contaminated territories: A case study of soils in primorsky krai. Sustainability. 17, 2369.

50. Ankita Sharma, Vivek Sharma, Divya Jain and Sudesh Kumar. (2025) Harnessing Hydroxyapatite: A Review on Synthesis and Green Solution for Cadmium and Lead Contamination in Wastewater. Current Green Chemistry.

51. Elvis O. Lopez , Pablo L. Bernardo, Noemi R. Checca, Andr'e L. Rossi, Alexandre Mello, Donald E. Ellis, Alexandre M. Rossi, Joice Terra. (2022)Hydroxyapatite and lead-substituted hydroxyapatite near-surface structures: Novel modelling of photoemission lines from X-ray photoelectron spectra. Applied Surface Science 571, 151310.

52. Kazuki Hamada, Masahiko Katoh. (2022)Formation of pyromorphite by hydroxyapatite during lead migration in soil with different phosphorus sorption abilities. Soils and Foundations Volume 62, Issue 6, 101241..

..